Accounting for O_2 absorption in ionospheric UV volume emission rate tomography

S. A. Kalashnikova, E. S. Andreeva, A. M. Padokhin

Lomonosov Moscow State University, Faculty of Physics, Moscow, 119991, Russia

E-mail: padokhin@physics.msu.ru

Abstract. This paper presents the modelling results on peculiarities and importance of including thermospheric extinction within the UV ionospheric tomography problem. O_2 absorption and its influence on tomographic reconstructions of OI 135.6 nm volume emission rate in nighttime ionosphere are considered based on NRLMSIS-00 and NeQuick2 models. Iterative solvers of ART family with constraints are used for tomographic reconstructions. It is shown that when scanning directions whose perigee is less than 200 km are included in the tomographic problem, neglecting of O_2 Schumann-Runge absorption leads to the destruction of the solution with pronounced periodic latitudinal artifacts. Excluding those rays in turn leads to narrowing of possible height region as well as to decreasing of horizontal resolution of reconstructions. At the same time, it is shown that using even significantly altered model for O_2 absorption (for example for solar maximum instead of solar minimum) does not seriously influence results of tomographic reconstructions while still causes latitudinal artifacts. It is caused by negligible absorption of UV nightglow at heights greater than 200 km where significant variations of O_2 concentrations with solar and geomagnetic activity are observed.

Accepted: 15.09.2020
DOI: 10.21046/2070-7401-2020-17-6-153-158

1. Introduction

Using ultraviolet (UV) airglow to study ionospheric F-region was described in the late 1960s and early 1970s. Early space experiments [1, 2] revealed two main mechanisms of nighttime ionospheric UV airglow: O^+ and e^- radiative recombination and oxygen ion-ion neutralization [3]. Later experiments in mid-latitudes showed that radiative recombination is the predominant mechanism of the nighttime OI 135.6 nm emission [4]. Remote sensing of F-region electron density using UV oxygen nightglow was successfully demonstrated in [5–7].

In the last two decades, tomographic approach has been actively applied to reconstruct 2D and 3D distributions of electron density or volume emission rate in ionospheric F-region according to satellite UV spectrometry data [8–12]. Moreover, unlike ionospheric radiotomography (see for example [13]), where the observation operator depends only on the geometry of the problem and the basis expansion of the unknown parameter (electron density), in the case of UV tomography this operator also depends on the extinction in the medium [11], which must be determined independently. The present work is devoted to modelling various possibilities of accounting for thermospheric extinction in the problem of tomographic reconstruction of the nighttime ionosphere OI 135.6 nm volume emission rate based on the nadir and limb UV spectrometry data from a polar low-orbit satellite (LEO).

2. UV volume emission rate tomography problem modelling

The idea of UV ionospheric tomography based on nadir and limb measurements of nightglow intensity onboard purely polar LEO is to reconstruct the latitude-altitude distribution of the volume emission rate of the chosen emission along the satellite track. In this article only nighttime OI 135.6 nm emission is considered. Its intensity I_k along the scanning direction l_k is determined by:

$$\int_{l_k} \varepsilon(\boldsymbol{r}) \cdot \exp\left(- \int_{l_k(r)} \rho(\mathbf{r}')\, \mathrm{d}l' \right) \mathrm{d}l = 4\pi I_k, \tag{1}$$

where $\varepsilon(\mathbf{r})$ is the volume emission rate of the OI 135.6 nm nightglow and exponential function in integral accounts for thermospheric extinction, with the power of exponent being optical depth. Note that the OI 135.6 nm volume emission rate is determined by electron density $[e]$, ion $[O^+]$ and atomic $[O]$ concentrations [5]:

$$\varepsilon = \frac{k_1 k_2 \beta_{1356} [O] \cdot [e] \cdot [O^+]}{k_2 [O^+] + k_3 [O]} + \alpha_{1356} [e] \cdot [O^+], \tag{2}$$

where the coefficients of the reactions are approximately $k_1 = 1.3 \cdot 10^{-15}$ cm^3/s, $k_2 = 1.0 \cdot 10^{-7}$ cm^3/s, and $k_3 = 1.4 \cdot 10^{-10}$ cm^3/s and the fraction of the neutralization reaction resulting in the precursor state (O^5S) for the 135.6 nm emission is $\beta_{1356} = 0.54$; the radiative recombination rate $\alpha_{1356} = 7.5 \cdot 10^{-13}$ cm^3/s at 1160 K. For modelling purposes ε in F-region can be easily obtained from (2) using $[O]$ from NRLMSIS-00 [14] and $[O^+] \approx [e]$ from NeQuick2 [15].

Thermospheric extinction for 135.6 nm emission in (1) is mostly determined by O_2 Schumann-Runge absorption and resonant scattering by O along the line of sight, latter process being much more difficult to model. In this work only O_2 absorption contribution to extinction is considered, so ρ in (1) can be presented in form:

$$\rho = \sigma [O_2], \tag{3}$$

where $\sigma = 7.3 \cdot 10^{-18}$ cm^2 is O_2 absorption crossection for 135.6 nm emission according to [16] and $[O_2]$ can be easily obtained from NRLMSIS-00.

In this work 135.6 nm nightglow intensities I_k are modelled for UV-spectrometer, located onboard purely polar LEO satellite, with orbit height 850 km. The instrument provides Earth's limb scans (each scan takes 92 s) in the orbit plane for angles [26.5–10.5°] below local horizon. Moreover, the instrument provides one nadir measurement each 22 s. These conditions determine the system of scanning directions l_k in forward model (1) presented in figure 1. Considered experimental geometry corresponds well with operation of SSUSI/SSULI instruments [17] onboard DMSP satellites.

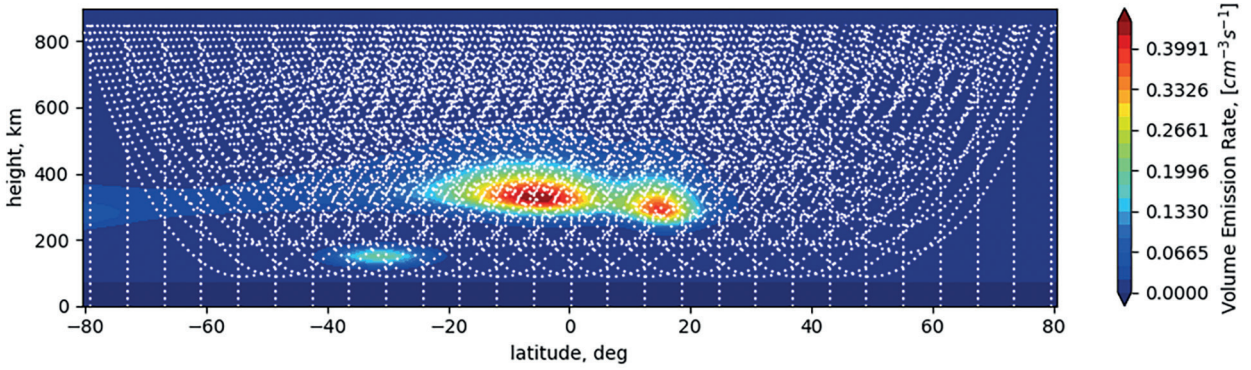

Figure 1. Model of latitudinal cross section (along 0°E) of nighttime thermospheric OI 135.6 nm volume emission rate, November 7, 2007 (22 UT). White dots represent nadir and limb scanning directions from polar LEO.

Nightglow intensities I_k obtained in the forward model act as an input data for tomographic inversion of ε distribution. The following inversion algorithm is used. The system of Fredholm integral equations of the first kind (1) is discretized by decomposition of the sought volume emission rate over finite basis. The unknown coefficients of basis expansion are volume emission rate values in the nodes

of the regular latitude-height grid and basis functions are chosen to provide bilinear interpolation of the sought volume emission rate within each cell of the grid. This procedure results in the system of linear algebraic equations (SLE) with sought vector representing volume emission rate values at each node of the grid, matrix elements being product of extinction coefficient and geometric factor for current scanning direction within current grid cell, and right hand side being nightglow intensities. In this work regular grid with cell dimensions (15 km height×2° latitude) is used. Figure 1 presents the reconstructed area. The resulting SLE is solved using iterative algebraic reconstruction technique (ART), which converges to normal solution relative to initial guess, which is set to zero. To ensure that ART iterations converge smoothly to a physically reasonable solution, the regularization in the form of Laplacian constraints is used between iterations, see [12] for details.

The following section represents results of modelling UV volume emission rate tomography problem with different variants of accounting for thermospheric O_2 absorption.

3. Modelling results

To model nighttime height-latitude distribution of OI 135.6 nm volume emission rate NeQuick2 and NRLMSIS-00 data for November 7, 2007 22 UT along 0° E longitude were chosen. This day is characterized by low solar and geomagnetic activity ($F10.7 = 66.9$ s.f.u., $K_p = 2$). Over NeQuick2 and NRLMSIS-00 background one additional irregularity at height 150 km was introduced into model to study tomographic inversion performance in height region, where absorption plays significant role. The resulting model distribution of ε used in the forward model is presented in figure 1 along with scanning directions.

Solid line in the left panel of figure 2 represents NRLMSIS-00 height profile of $[O_2]$ used in the forward model. Middle and right panels of figure 2 demonstrate the influence of O_2 absorption for different scanning directions. Note, that for large angles of limb scanning (e.g. 26.1° and 25.7° below horizon) corresponding to perigees ~150 km full absorption is observed for UV radiation originated in cells with angular distances from satellite greater than scanning angle. Thus, only half of the cells along those scanning directions effectively contribute to observed UV intensity. The same is valid for nadir scanning direction. For scanning directions with smaller angles below horizon influence of absorption is less pronounced and more cells along line of sight start to contribute to observed UV intensity.

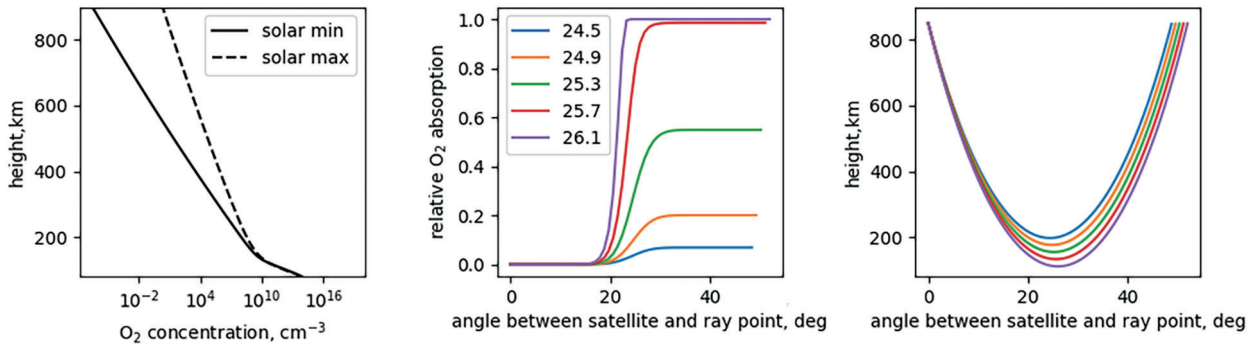

Figure 2. Height profiles of thermospheric O_2 concentrations for solar maximum and solar minimum conditions (left); relative O_2 absorption (middle) and corresponding ray trajectories (right) for different limb scanning angles.

Thus, accounting for O_2 absorption should be very important when including rays with small perigee heights within tomographic inversion. To test this importance four scenarios were considered. In the first scenario matrix of SLE was constructed using full system of scanning directions (nadir and limb with low rays included, see figure 1) neglecting O_2 absorption. In the second scenario only limb scanning directions with angles smaller than 24.5° were used (rays less affected by absorption). O_2 absorption was also neglected. Third and fourth scenarios both used O_2 absorption models when constructing SLE matrices. Third scenario served as a reference and used the very same $[O_2]$ distribution for absorption modelling as in forward model (figure 2, left panel, solid curve). Fourth scenario used altered O_2 distribution for higher solar and geomagnetic activity ($F10.7 = 275.4$ s.f.u., $K_p = 8$ see

figure 2, left panel, dashed curve). In all four scenarios right hand side was computed using correct $[O_2]$ distribution.

Figure 3 shows results obtained in first two scenarios, where thermospheric absorption is neglected. Left panels show results of the tomographic reconstruction of the model from figure 1, right panels — corresponding relative errors. Note that in both scenarios additional irregularity at 150 km height is not resolved. In first case this is the result of almost full absorption of UV nightglow originated in this region on the way to the satellite height which is not taken into account in observation matrix. In the second case it is the result of excluding all scanning rays passing through this region. Since the right hand side (measured UV intensity) is computed in forward model with account for absorption, tomographic inversion, which is not taking into account absorption, will underestimate volume emission rate along rays penetrating deeper into lower ionosphere, where $[O_2]$ is large, and compensate it by overestimating volume emission rate along adjacent rays. Since such rays are repeated almost uniformly in consecutive scans as the satellite moves along its orbit, latitudinal periodic modulation in reconstructed volume emission rate is observed (figure 3 top left panel). This effect is even more pronounced in relative error plot (figure 3 top right panel). Such latitudinal periodic modulation is obviously less but still clearly pronounced in the results of second scenario (figure 3 bottom), where vertical and deep penetrating oblique rays, highly affected by absorption, are excluded in tomographic inversion. These results correspond well with those presented in [11].

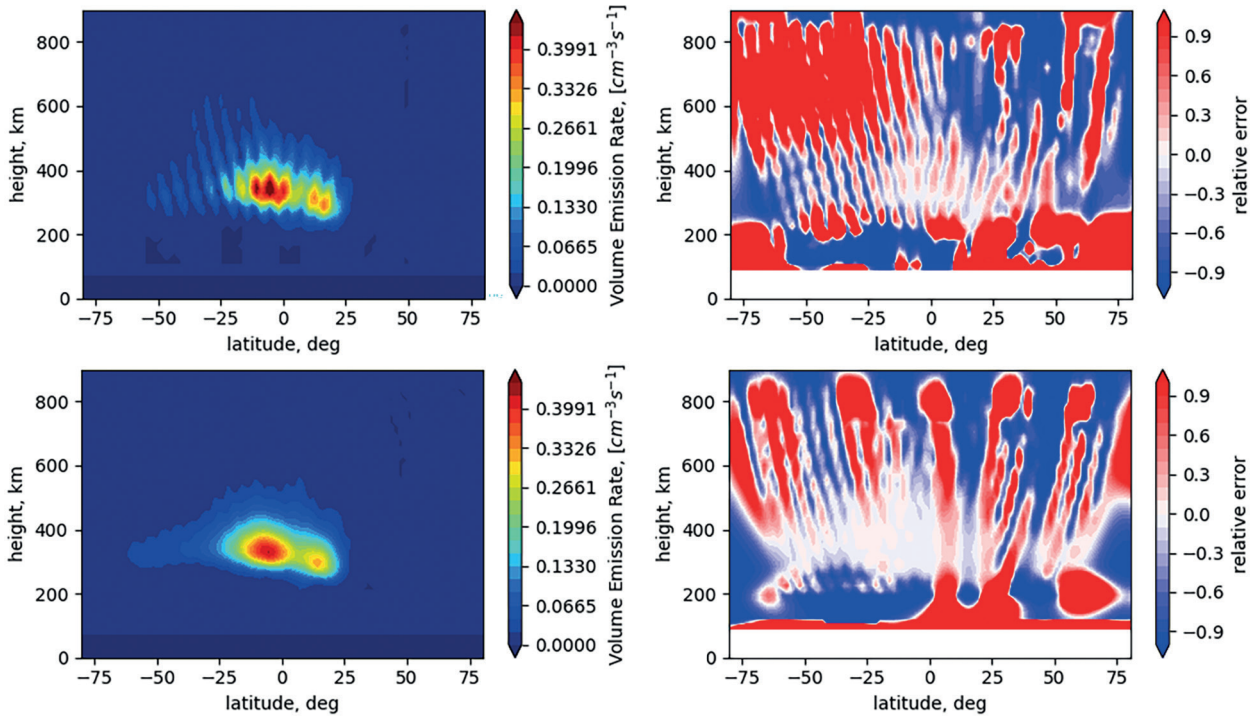

Figure 3. Tomographic reconstructions (left) of nighttime thermospheric OI 135.6 nm volume emission rate model (see figure 1) and corresponding errors (right) when thermospheric extinction is neglected. Top panel — full system of scanning directions; bottom panel — reduced system of scanning directions with perigees greater than 200 km.

Figure 4 shows results obtained in last two scenarios, where thermospheric absorption is taken into account using different $[O_2]$ distributions. Left panels again show results of the tomographic reconstruction of the model from figure 1, right panels — corresponding relative errors. Note, that in contrary to first two scenarios, additional low altitude irregularity is well resolved here. Both scenarios show reasonable reconstruction errors in areas, where volume emission rate is relatively high (F-layer maximum), which increase in the areas, where volume emission rate is low. Latitudinal periodic artifacts are less pronounced (among all considered cases) in reference third scenario, where correct O_2 distribution was used in tomographic inversion, where they are mostly due to discretization error. Using even significantly altered O_2 profile (e. g. solar maximum conditions instead of solar minimum)

to account for absorption still provides the possibility to reconstruct structures in lower ionosphere, which is impossible when neglecting absorption. Latitudinal periodic artifacts in this case may be the signature of how far is absorption model used in tomographic inversion from the one, realized in thermosphere.

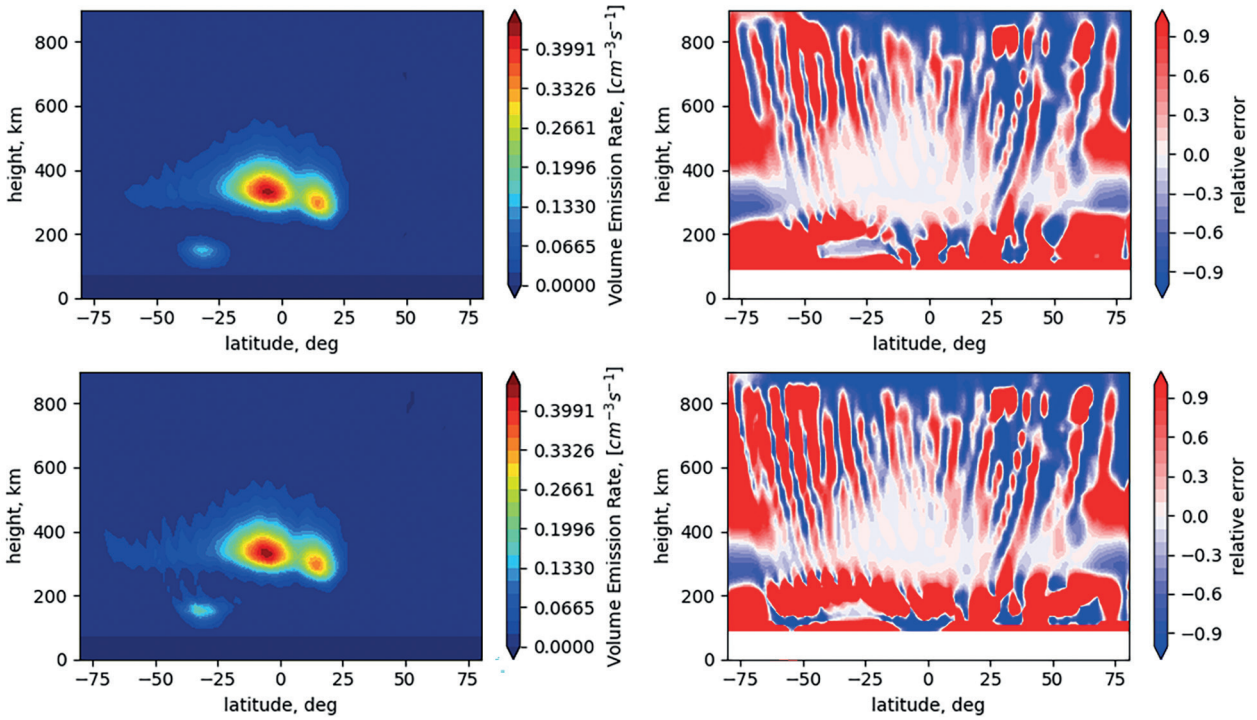

Figure 4. Tomographic reconstructions (left) of nighttime thermospheric OI 135.6 nm volume emission rate model (see figure 1) and corresponding errors (right) with account for O_2 absorption. Top panel — correct thermospheric O_2 profile; bottom panel — altered thermospheric O_2 profile.

4. Conclusions

Ionospheric UV tomography is a powerful tool for remote sensing of upper atmosphere. Compared to radiotomography it requires accounting for thermospheric extinction in inversion procedure. Results of the modelling show, that even neglecting thermospheric extinction, overall morphology of volume emission rate in upper ionosphere can be reconstructed, although loosing information about lower ionosphere. Moreover, latitudinal periodical artifacts are present in reconstructions in this case. Using some reasonable model for thermospheric extinction in tomographic inversion could increase the capabilities of the method in lower ionosphere, while observed latitudinal periodic artifacts may be used as an indicator of how well modeled thermospheric extinction reflects the actual one. Note, that presented results are for nighttime only and took into account only absorption part of thermospheric extinction. Additional modelling is needed for tomographic inversions in daytime ionosphere and accounting for resonant scattering contribution to thermospheric extinction.

Acknowledgements

Authors would like to thank Community Coordinated Modeling Center (CCMC) for NRLMSIS-00 source code, Bruno Nava (ICTP) for NeQuick2 source code and acknowledge financial support of the Russian Foundation for Basic Research (Project No. 19-05-00941).

5. References

[1] Hicks G. T., Chubb T. A., Equatorial aurora/airglow in the far ultraviolet, *J. Geophysical Research*, 1970, Vol. 75(31), pp. 6233–6248.

[2] Barth C. A., Schaffner S., Ogo 4 spectrometer measurements of the tropical ultraviolet airglow, *J. Geophysical Research*, 1970, Vol. 75(22), pp. 4299–4306.

[3] Knudsen W. C., Tropical ultraviolet nightglow from oxygen ion-ion neutralization, *J. Geophysical Research*, 1970, Vol. 75(19), pp. 3862–3866.

[4] Brune W. H., Feldman P. D., Anderson R. C., Fastie W. G., Henry R. C., Midlatitude Oxygen Ultraviolet Nightglow, *Geophysical Research Letters* 1978, Vol. 5(5), pp. 383–386.
[5] Tinsley B. A., Bittencourt J. A., Determination of F region height and peak electron density at night using airglow emissions from atomic oxygen, *J. Geophysical Research* 1975, Vol. 80(16), pp. 2333–2337.
[6] Meier R. R., Ultraviolet spectroscopy and remote sensing of the upper atmosphere, *Space Science Reviews*, 1991, Vol. 58, 185 p.
[7] Dymond K. F., Thonnard S. E., McCoy R. P., Thomas R. J., An optical remote sensing technique for determining nighttime F region electron density, *Radio Science*, 1997, Vol. 32(5), pp. 1985–1996.
[8] Dymond K. F., Thomas R. J., An algorithm for inferring the two-dimensional structure of the nighttime ionosphere from radiative recombination measurements, *Radio Science*, 2001, Vol. 36(5), pp. 1241–1254.
[9] DeMajistre R., Paxton L. J., Morrison D., Yee J. H., Goncharenko L. P., Christensen A. B., Retrievals of nighttime electron density from Thermosphere Ionosphere Mesosphere Energetics and Dynamics (TIMED) mission Global Ultraviolet Imager (GUVI) measurements, *J. Geophysical Research: Space Physics* 2004, Vol. 109(A5), A05305, 14 p.
[10] Comberiate J. M., Kamalabadi F., Paxton L. J., A tomographic model for ionospheric imaging with the Global Ultraviolet Imager, *Radio Science*, 2007, Vol. 42, RS2011, 12 p.
[11] Hei M. A., Budzien S. A., Dymond K. F., Nicholas A. C., Paxton L. J., Schaefer R. K., Groves K. M. Ionospheric-thermospheric UV tomography: 3. A multisensor technique for creating full-orbit reconstructions of atmospheric UV emission, *Radio Science*, 2017, Vol. 52, pp. 896–916.
[12] Nesterov I. A., Padokhin A. M., Andreeva E. S., Kalashnikova S. A., Modeling the problem of low-orbital satellite UV-tomography of the ionosphere, *Moscow University Physics Bulletin*, 2016, Vol. 71, pp. 329–338.
[13] Kunitsyn V. E., Nesterov I. A., Padokhin A. M., Tumanova Y. S., Ionospheric radio tomography based on the GPS/GLONASS navigation systems, *J. Communications Technology and Electronics*, 2011, Vol. 56, pp. 1269–1281.
[14] Picone J. M., Hedin A. E., Drob D. P., Aikin A. C., NRLMSISE-00 empirical model of the atmosphere: Statistical comparisons and scientific issues, *J. Geophysical Research: Space Physics*, 2002, Vol. 107(A12), pp. SIA 15– SIA 16.
[15] Nava B., Coïsson P., Radicella S., A new version of the nequick ionosphere electron density model, *J. Atmospheric and Solar-Terrestrial Physics*, 2008, Vol. 70, pp. 1856–1862.
[16] Watanabe K., Inn E. C. Y., Zelikoff M., Absorption Coefficients of Oxygen in the Vacuum Ultraviolet, *The J. Chemical Physics*, 1953, Vol. 21(6), 1026.
[17] McCoy R. P., Dymond K. F., Fritz G. G., Thonnard S. E., Meier R. R., Regeon P. A., Special sensor ultraviolet limb imager: An ionospheric and neutral density profiler for the defense meteorological satellite program satellites *Optical Engineering* 1994, Vol. 33(2), pp. 423–429.